

Tailoring the Mechanical and Electrochemical Properties of an Artificial Interphase for High-Performance Metallic Lithium Anode

Yipeng Sun, Maedeh Amirmaleki, Yang Zhao, Changtai Zhao, Jianneng Liang, Changhong Wang, Keegan R. Adair, Junjie Li, Teng Cui, Guorui Wang, Ruying Li, Tobin Filleter,* Mei Cai,* Tsun-Kong Sham,* and Xueliang Sun*

Lithium metal is regarded as the “Holy Grail” of anode materials due to its low electrochemical potential and high theoretical capacity. Unfortunately, its unstable solid electrolyte interphase (SEI) leads to low Coulombic efficiency (CE) and serious safety issues. Herein, a hybrid nanoscale polymeric protective film with tunable composition and improved stiffness is developed by incorporating aluminum crosslinkers into the polymer chains. The Li plating/stripping process is regulated through the protective coating and the dendrite growth is effectively suppressed. Promisingly, the protected Li can deliver stable performance for more than 350 h with a cycling capacity of 2 mAh cm⁻² without a notable increase in overpotential. Moreover, a stable charge/discharge cycling in Li–O₂ batteries with the protected Li can be maintained for more than 600 h. This work provides guidance on the rational design of electrode interfaces and opens up new opportunities for the fabrication of next-generation energy storage systems.

Li-S, Li-air and all-solid-state batteries.^[1] It has attracted significant research interests due to its high theoretical specific capacity (3860 mAh g⁻¹), which is more than ten times the value of commercial graphite anode (372 mAh g⁻¹). In addition, the redox potential of Li (–3.04 V vs the standard hydrogen electrode) is the lowest among all the anode material candidates.^[2] Therefore, the Li metal anode, in principle, can deliver an ultra-high energy density for the application of next-generation batteries. However, several serious challenges concerning the safety and cyclability of Li metal anodes have hindered the practical application.^[3] Li dendrite formation, a major concern during electrodeposition, can penetrate the separator and trigger short circuits,

1. Introduction

Lithium (Li) metal is widely believed as one of the most promising anode materials for next-generation batteries, including


Y. Sun, Dr. Y. Zhao, Dr. C. Zhao, J. Liang, Dr. C. Wang, K. R. Adair, J. Li, R. Li, Prof. X. Sun

Department of Mechanical and Materials Engineering
University of Western Ontario
London, Ontario N6A 5B9, Canada
E-mail: xsun@eng.uwo.ca

Y. Sun, Prof. T.-K. Sham
Department of Chemistry
University of Western Ontario
London, Ontario N6A 5B7, Canada
E-mail: tsham@uwo.ca

M. Amirmaleki, T. Cui, Dr. G. Wang, Prof. T. Filleter
Department of Mechanical and Industrial Engineering
University of Toronto
Toronto M5S 3G8, Canada
E-mail: filleter@mie.utoronto.ca

Dr. M. Cai
General Motors R&D Center
Warren, MI 48090-9055, USA
E-mail: mei.cai@gm.com

 The ORCID identification number(s) for the author(s) of this article can be found under <https://doi.org/10.1002/aenm.202001139>.

DOI: 10.1002/aenm.202001139

giving rise to serious safety concerns. During electrochemical dissolution, a layer of “dead Li”, which formed owing to the loss of electrical contact from the bulk Li, impedes the electron/ion transport at the interface between Li and electrolyte. Moreover, due to the high reactivity of Li, side reactions with the electrolyte promote the formation of inhomogeneous solid electrolyte interphase (SEI) components. The large volume expansion induced by Li plating yields a fractured interface and further consumption of the electrolyte to form new SEI. The continuous degradation of electrolyte and reformation of SEI is an irreversible process resulting in capacity loss and low coulombic efficiency (CE).^[4]

In the electrochemical plating process, the nucleation and growth of dendritic Li are closely related to the properties of the SEI.^[5] As a result, the SEI plays an extremely important role on the morphology of Li deposits and influences the cycling performance of Lithium Metal Batteries (LMBs). SEI on Li metal is a nanoscale layer composed of various organic and inorganic components.^[6] The formation of SEI is an irreversible process that consumes both Li and organic electrolyte, thus leading to a decrease in CE. Meanwhile, direct contact between Li and electrolyte is effectively blocked by the SEI, leading to the suppression of further side reactions. However, the naturally formed SEI layer of Li metal is unstable due to its heterogeneous composition and low modulus.^[7] The relative infinite volumetric change of Li metal in plating/stripping

requires an SEI layer with excellent mechanical properties, especially for high cycling rates and capacities. Therefore, the development of a robust artificial SEI is believed to be of great significance for the practical application of alkali metal anodes.^[8]

To date, there are two strategies to stabilize the SEI for Li metal: i) an in situ approach by electrolyte modification and ii) an ex situ approach by pre-treatment of the Li surface. On one hand, as an in situ approach, optimization of Li salt concentration and modification of electrolyte additives (e.g., CsPF₆,^[9] fluoroethylene carbonate,^[10] and dual salts^[11]) have been reported to facilitate the formation of stable SEI component during the electrochemical process. On the other hand, various coatings (e.g., Li₃PS₄,^[12] Li₃PO₄,^[13] and polymers^[14]) have been applied on Li via different treatments as ex situ approaches. Although the electrochemical performance can be improved by both approaches, SEI with homogeneous composition, well-controlled thickness and extraordinary stability over long-term cycling is still rarely reported. In recent years, protective coatings deposited by atomic layer deposition (ALD) or molecular layer deposition (MLD), including inorganic metal oxide (such as Al₂O₃^[15] and ZrO₂^[16]) and organic polymers (such as alucone and polyurea), have been adopted for Li metal anode as artificial SEI with precise control over thickness and conformity.^[17] MLD coatings are believed to be more effective compared with ALD metal oxides due to their high flexibility. However, there are still challenges remaining for MLD films as artificial SEI for Li metal anodes. First, stable electrochemical performances at high current density and high capacity with thin coatings are rarely reported.^[18] Second, although polymer-based films are flexible, they normally have limited mechanical strength. Meanwhile, excellent mechanical properties of protective films are required for high rate performances. Finally, tunable composition of the films by ALD/MLD and investigation on the influence of composition toward electrochemical cycling are still lacking.

To address the above challenges, inspired by inorganic fillers for mechanical enhancement of polymers, we report a hybrid polyurea (HPU) film with tunable composition and improved stiffness as an artificial SEI for Li metal by introducing trimethylaluminum (TMA) as a crosslinker into the polymer chains. Atomic force microscopy (AFM)-based film deflection measurements reveal enhanced stiffness in the HPU film. The dendrite formation is effectively suppressed by this artificial SEI, and Li plating/stripping process also can be regulated owing to its electronic insulation nature.^[19] As a result, the electrochemical performances of Li metal anode are significantly improved with the HPU coatings, compared with bare Li and pure polyurea (PU) coated Li. The optimized thickness (≈30 nm) of 10 MLD cycles of HPU on Li metal (Li@H10) can prevent the formation of dendrites and achieve uniform Li plating/stripping, resulting in prolonged lifetime at a high current density of 5 mA cm⁻² in symmetric cells. Furthermore, Li–O₂ batteries using Li@H10 can be operated for more than 600 h, and Li–LiFePO₄ batteries using Li@H10 show almost no capacity fading after 300 charge/discharge cycles. Our concept opens new windows toward realizing stable ultra-thin hybrid films as protective layers for high performance and long-life Li metal anodes.

2. Results and Discussion

The MLD procedure for polyurea (PU) using ethylenediamine (ED) and 1,4-phenylene diisocyanate (PDIC) as precursors was previously reported by our group.^[20] To tune the mechanical properties of the pure polyurea, TMA as Al-crosslinkers have been introduced into the PU films to produce the HPU coatings. One single hybrid MLD cycle is defined by the sequence of TMA-ED-PDIC-ED. The reaction mechanism of MLD HPU is shown in Figure S1 in the Supporting Information, in which dative Al–N bonds are formed by the reaction between TMA and ED, and urea bonds are formed by the reaction between isocyanate groups from PDIC and amine groups from ED. Furthermore, the amount of Al-crosslinkers in the HPU films are controlled with different pulse numbers of TMA in the MLD cycles. For the sequence of TMA-ED-PDIC-ED, it is denoted as 1/4 Al as there is 1 pulse of TMA in a total of 4 pulses. Similarly, for other TMA amounts, the pulses of TMA in the total pulses for hybrid polyurea were 1 over 4, 8, and 16, denoted as H10 1/4 Al, H10 1/8 Al, and H10 1/16 Al, respectively. Detailed experimental procedures for various amount of Al can be found in the supporting information. A quartz crystal microbalance (QCM) monitored the growth of hybrid coatings as shown in Figure S2 in the Supporting Information. The QCM data showed MLD deposition with sequential and stepwise reaction manners from the hybrid polyurea with Al content in the range of 0–1/4 Al (Figure S2A–F, Supporting Information). However, when further increasing the Al amount to 3/8, there was a decrease in the mass change in the QCM data, suggesting no film growth was achieved. This can be explained by the saturation of functional groups in ED, which cannot further react with more TMA pulses. Therefore, QCM data indicated that the highest number of pulses of TMA in polyurea is 1 in a total 4 precursor pulses. The relative concentrations of Al in HPU coatings with 1/4 Al, 1/8 Al, and 1/16 Al were confirmed by Inductively Coupled Plasma Mass Spectrometry (ICP-MS) testing (Figure S3, Supporting Information).

The 1/4 Al in HPU films are chosen as typical examples for surface characterization. 10 MLD cycles of 1/4 Al in HPU were conducted on fresh Li foil (denoted as Li@H10) as shown in Figure 1A. Time-of-flight secondary ion mass spectrometry (TOF-SIMS) was performed on Li@H10 to obtain a detailed depth profile of the MLD coating by collecting the information from various secondary ions. 3D reconstruction of total ions clearly showed the distribution of secondary ions and illustrated the hybrid coating on the surface of Li metal (Figure 1B). In Figure 1C, CN⁻ and NCO⁻ ions were generated from the urea bond of the polymer chains, while AlNH₂⁻ ions were generated from Al-crosslinkers in the HPU. The signal from Li⁻ was initially low and was observed to rise thereafter, suggesting that the bulk Li started to emerge upon the removal of HPU layers by sputtering. The concentrations of all the three ions (CN⁻, NCO⁻, and AlNH₂⁻) decreased with longer sputter time and became leveled after prolonged time following a similar trend. Taking NCO⁻ as representative ions from the coating, the signal became leveled after 150 s, which indicated the complete ion etching through the HPU layer. Film thickness can be estimated by the sputtering rate multiplied by the sputtering time. The result indicates a coating thickness of ≈30 nm for Li @H10

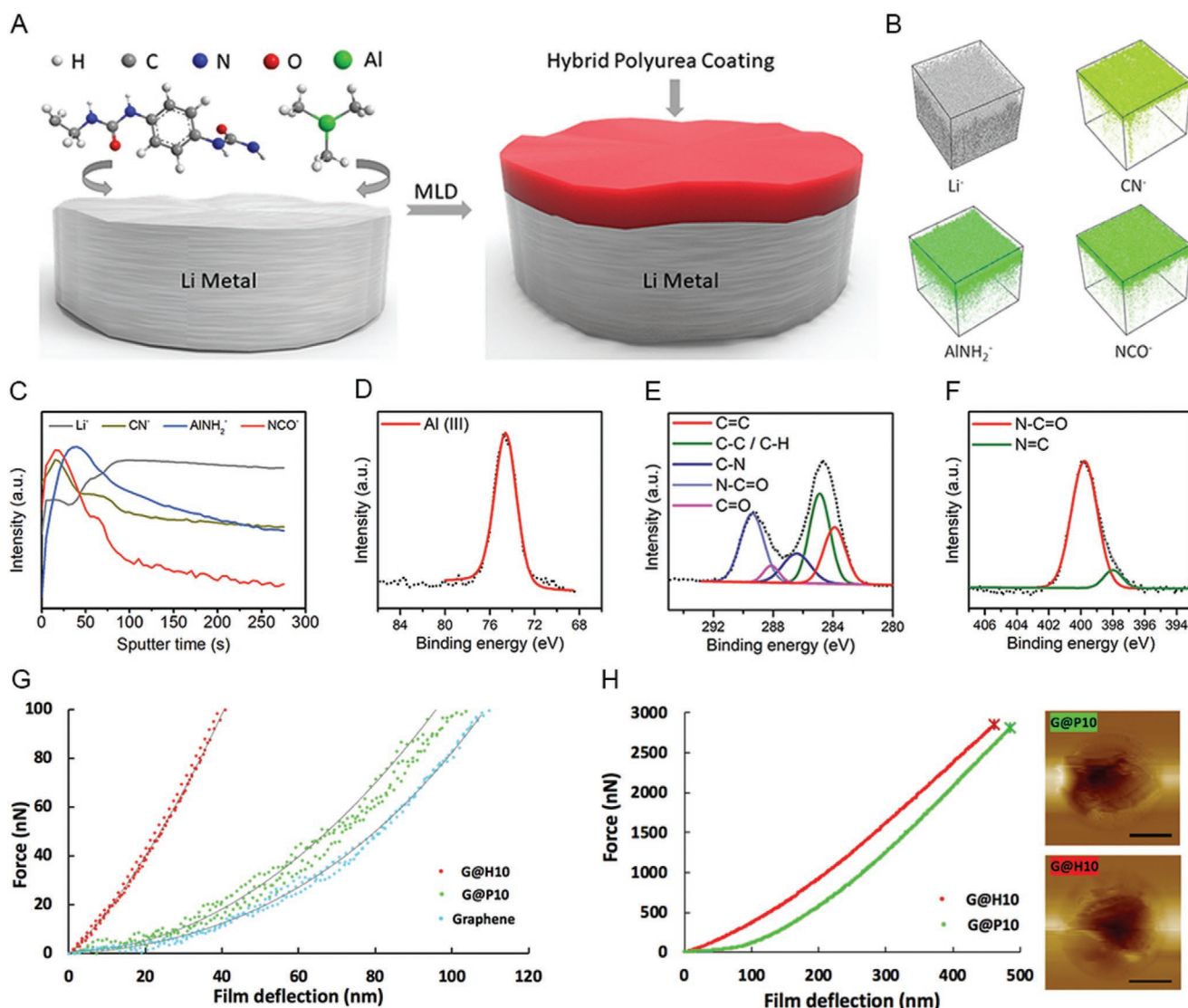


Figure 1. A) Schematic showing the synthesis procedure of the MLD hybrid polyurea coating for enhanced mechanical property. B) 3D reconstruction of the various secondary ions after Bi₃⁺ sputtering. C) TOF-SIMS profile depth profile of some typical secondary ions from Li@H10. High-resolution XPS spectra of Li@H10 for D) Al 2p, E) C 1s, and F) N 1s. G) Force–deflection (F – δ) curve of freestanding films deflected within an elastic regime. H) Left Force–deflection curve of the films deflected to failure (stars indicate failure point), right AFM topography image of failed films with scale bars representing 1 μ m. Presented F – δ curves were representative of at least ten independent freestanding films measured for each group.

from a 0.2 nm s⁻¹ sputter rate and 150 s. The thickness is in line with the growth rate reported previously by our group.^[20] It is worth mentioning that the calculation of thickness from TOF-SIMS is just an approximate estimation since the surface of Li is not perfectly smooth. X-ray photoelectron spectroscopy (XPS) was also conducted to study the chemistry at the surface of Li@H10 (Figure 1D–F). In Al 2p spectrum (Figure 1D), the peak at 73.6 eV is assigned to a valence of +3 in Al-crosslinkers.^[21] Various states of C were observed from C 1s spectrum in Figure 1E, including C=C, C–C, C–H, C=N, and C=O from the polyurea chains in the range from 283.9 to 289.4 eV. The bonding between C and N was also confirmed by the N 1s spectrum in Figure 1F, which was consisted of mainly N–C=O at 399.7 eV from the urea bond and a small percentage of N=C at 398.0 eV from the isocyanate end groups.

Various MLD cycles (10, 25, and 50 cycles) of HPU with 1/4 Al were coated on Li foils to study the effects of coating thickness. TOF-SIMS results demonstrated an increasing thickness from 10 cycles to 50 cycles from 3D reconstruction of various secondary ions (Figure S4A–C, Supporting Information). There were clear layers of HPU coatings on Li for all three of the MLD cycles and the detailed depth profiles showed similar trends of the secondary ions with different thicknesses (Figure S4D–F, Supporting Information). These results demonstrated the thickness of HPU coating on Li can be reliably controlled by simply adjusting the number of MLD cycles.

To gain a further understanding on the chemical and structural information of the HPU coating, near-edge X-ray absorption fine structure (NEXAFS) spectroscopy was performed as shown in Figure S5 in the Supporting Information. In the C

K-edge spectrum, a stronger peak at 285.0 eV was assigned to the transition of C 1s (C–H) \rightarrow $1\pi^*_{C=C}$ from the phenyl group, while a weaker peak at 286.2 eV was corresponded to the transition of C 1s (C–R) \rightarrow $1\pi^*_{C=C}$ from the bonding between phenyl carbon and amide groups.^[22] The peak at 286.2 eV was shifted to higher energy due to the electron-withdrawing nature of amide group.^[23] The C 1s (C=O) \rightarrow $1\pi^*_{C=O}$ transition occurs at 289.1 eV, and the shoulder on its left was assigned to the C 1s \rightarrow $2\pi^*$ (b_{2g}) transition in benzene ring-type structures. In the N K-edge spectrum (Figure S5B, Supporting Information), the peak at 402.0 eV was assigned to N 1s (C=O) \rightarrow π^* transition.^[24] A broad peak at 408.4 eV was believed to be related to 2 strong near continuum resonances of $\sigma^*_{N-C=O/N-Ph}$ character, and its shoulder at 405.0 eV matched the high energy orbital on the phenyl ring.

The mechanical properties of MLD HPU films were investigated by conducting atomic force microscopy (AFM)-based film deflection measurements. To understand the influence of Al-crosslinker into PU films toward the mechanical properties, two groups of samples prepared with 10 cycles of MLD HPU (G@H10) and MLD PU (G@P10) were deposited over circularly suspended single-layer graphene, as a supporting layer, on holey transmission electron microscopy (TEM) grids. Tapping mode AFM topography imaging was first performed to find damage-free films, and then AFM deflection testing was conducted at the center of the suspended film using a diamond AFM tip following a previously reported method.^[25] The elastic behavior of films was studied by deflecting the film with a maximum normal force of 100 nN at a constant displacement rate of $10\ \mu\text{m}\ \text{s}^{-1}$. After each loading, subsequent AFM topography imaging revealed no permanent deformation occurred to the film, ensuring testing within the elastic regime. Similar to our previous study,^[25] no sign of weak bonding or slippage was observed during the test in elastic regime. Figure 1G shows representative force-deflection ($F-\delta$) curves of the G@P10, G@H10, and graphene support layer. Based on a continuum mechanics analysis,^[26] the effective elastic moduli were determined as presented in Table S1 in the Supporting Information (see more details in the experimental section 3 of supporting information). The in-plane stiffness of the G@H10 was found to be higher than G@P10. In addition to elastic deflection testing, the films were also deflected to fracture to further investigate the mechanical failure behavior. Significant fracture of the films was identified by an abrupt force drop to or beyond 20% of the maximum force^[27] as shown with stars in Figure 1H, which is further confirmed by subsequent AFM imaging. The elastic and failure results showed that specifically, G@H10 films maintain the highest stiffness, from the slope of ($F-\delta$) curve, during the entire loading stage to failure. Interestingly, the G@P10 showed compliance (reciprocal of stiffness) in the elastic region ($<100\ \text{nm}$ deflection); however, the slope of $F-\delta$ curve was observed to significantly increase at higher forces and as such the film exhibited higher stiffness. For G@H10 the average slope of $F-\delta$ curve below 100 nN force was $2.93\ \text{nN}\ \text{nm}^{-1}$ and changed to $7.53\ \text{nN}\ \text{nm}^{-1}$ beyond 1000 nN force, while for G@P10 the average slope below 100 nN force was $1.33\ \text{nN}\ \text{nm}^{-1}$ and changed to $9.46\ \text{nN}\ \text{nm}^{-1}$ beyond 1000 nN force. The increased stiffness is likely due to strain hardening of PU induced by the alignment of the entangled

polymer network during plastic deformation.^[28] The lower change in stiffness of G@H10 films at higher forces is likely because the chains are already initially aligned and ordered parallel to the surface as shown in our previous work,^[20] therefore the work hardening effect is less evident. This indicates that additional Al-crosslinkers create a stiffer polymer structure and lowered stiffness hardening of the polymer under the AFM tip at higher forces due to the preferred alignment parallel to the substrate. It should however be noted that high stiffness alone cannot fully account for the observed improvements of HPU as compared to PU. Therefore, the electrochemical, chemical, and mechanical properties of the MLD PU and HPU layers are summarized in Table S2 in the Supporting Information, which indicates that an optimal interplay between the stiffness, strength, coating thickness, and ionic conductivity improves the resistance against dendrites formation and maximizes the stability of the Li metal batteries in this study.

2032-type symmetric cells with a configuration of Li/separators and electrolyte/Li were assembled to evaluate the electrochemical performance of Li metal anodes. Commercial electrolyte composed of 1 M LiPF₆ in 1:1:1 ethylene carbonate (EC)/diethyl carbonate (DEC)/dimethyl carbonate (DMC) was used as carbonate-based electrolyte. A comparison of the electrochemical performance of different Al amounts in HPU are shown in Figure S6 in the Supporting Information. At a current density of $5\ \text{mA}\ \text{cm}^{-2}$, all the Li metal anodes with HPU coatings showed improved cycling stability compared to bare Li in the electrochemical testing. Furthermore, HPU coatings with larger amount of Al exhibited much lower overpotential after 50 h. The overpotential of H10 with 1/4 Al was the lowest among all the anodes, suggesting that the optimum amount of Al in the HPU as coating for Li metal anode is 1/4. With the improved stiffness of Li@H10 confirmed by AFM-based film deflection measurements, its electrochemical performance in symmetric cells is optimized by tuning the amount of Al-crosslinkers. To understand the effects of coating thickness toward Li metal, Li@H5, Li@H10, Li@H25, and Li@H50 were used to assemble symmetric cells and tested for comparison (Figure S7, Supporting Information). There was a small overpotential of $\approx 150\ \text{mV}$ in the beginning in Li@H5, however, it increased quickly to above 250 mV in 100 cycles. The increase in overpotential indicated that with only 5 MLD cycles the Li metal was not fully covered and the SEI was still not stable. Among all the thicknesses, it can be observed that Li@H10 exhibited the lowest overpotential at $\approx 140\ \text{mV}$ after 100 cycles. The increase in overpotential was observed clearly when increasing MLD cycles to 25 and 50, suggesting that thick layer of HPU can hinder the Li ion transportation and cause higher polarization. The results shown in Figure S7 in the Supporting Information indicate that the optimum MLD cycles for Li metal anode is 10.

After the comparisons of both coating thickness and percentage of Al, Li@H10 as the optimized anode was used to assemble symmetric cells and electrochemically tested in comparison to 10 MLD cycles of pure PU coated Li metal anode (Li@P10), which was reported as the optimized PU coating in our previous work.^[18] When stripping/plating at a current of $2\ \text{mA}\ \text{cm}^{-2}$, the symmetric cell assembled using Li@P10 can run for more than 100 h with a small overpotential below

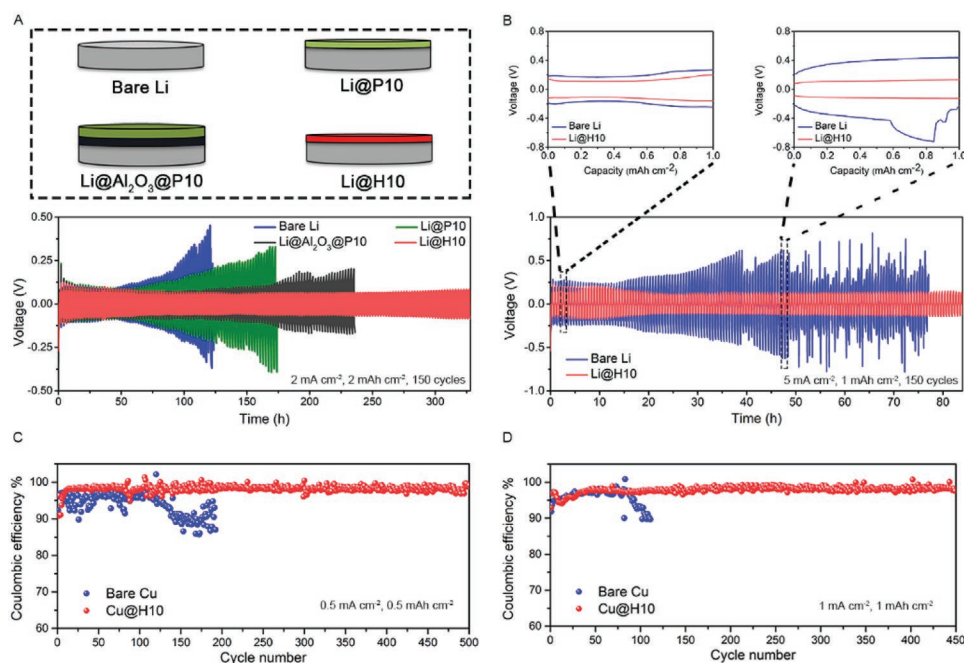


Figure 2. A) The overpotential of symmetric cells using bare Li, Li@P10, Li@Al₂O₃@P10, and Li@H10 at a current density of 2 mA cm⁻². B) A comparison of electrochemical performance of bare Li and Li@H10 in symmetric cells with detailed voltage profile in initial stage and late stage at a current of 5 mA cm⁻². Evaluation of Coulombic efficiency (CE) of bare Cu and Cu@H10 in Cu-Li cells at current densities of C) 0.5 mA cm⁻² and D) 1 mA cm⁻².

200 mV, exhibiting improved stability compared to bare Li, as shown in Figure 2A. More promisingly, Li@H10 retained an overpotential below 100 mV with minimal changes even after 350 h. Therefore, compared with PU coating, HPU coating demonstrated significantly enhanced protective effects toward Li. By contrast, the overpotential of bare Li quickly raised to ≈450 mV in 120 h, and a sudden drop then occurred as a sign of soft shorting after 122 h from beginning. The sharp increase in overpotential indicates the consumption of electrolyte due to its side reactions with Li, while it is clear the side reactions can be suppressed by MLD artificial SEI. To further investigate the differences between adding Al-crosslinkers in PU and adding a separate inorganic layer in PU, we also deposited a dual-layer coating composed of both PU and Al₂O₃ on Li (denoted as Li@Al₂O₃@P10, in which Al₂O₃ layer is in between Li and P10) to evaluate the electrochemical performance. In the dual-layer coating the Al₂O₃ was present in a separate layer instead of in the polymer chains. Li@Al₂O₃@P10 exhibited improved performance than Li@P10, but it still had undergone an obvious increase in overpotential after 150 h, whereas the overpotential of Li@H10 remained stable throughout the electrochemical testing. Therefore, it can be concluded that the SEI in Li@H10 is more robust than Li@Al₂O₃@P10, and more evidence is revealed by XPS which will be discussed later in this essay.

Figure 2B showed the cycling performance of Li@H10 which was cycled with an increased current density of 5 mA cm⁻² for a prolonged time. It is apparent that Li@H10 was able to be cycled stably and the overpotential was maintained at ≈150 mV after 150 plating/stripping cycles at a capacity of 1 mAh cm⁻². Flat and smooth charge/discharge curves of Li@H10 without noticeable fluctuation can be clearly observed in the detailed voltage profiles not only in the initial

stage but also after a large number of charge/discharge cycles. By contrast, the overpotential from bare Li raised rapidly above 600 mV in only 50 h and severe fluctuations in overpotential can be clearly seen in the following charge/discharge process. We also tested the symmetric cell using Li@P10 at the current of 5 mA cm⁻² for comparison. It showed a rapid increase in overpotential from ≈160 to ≈500 mV with a sign of short circuiting within 130 cycles (Figure S8, Supporting Information). Therefore, the cycling life of Li@H10 at the current of 5 mA cm⁻² is also prolonged compared to Li@P10. We further pushed the capacity to 3 mAh cm⁻² as it is closer to the practical application requirements of Li metal batteries (Figure S9, Supporting Information). Symmetric cells with Li@H10 can be cycled for 350 h with an overpotential below 100 mV while that with bare Li showed more than tripled overpotential after 350 h, indicating that the nanoscale coating of HPU on Li can improve the interfacial stability over repeated stripping/plating process in a long period. We summarized the cycling performances of artificial SEI protected Li metal in symmetric cells from reported literature in Table S3 in the Supporting Information. The HPU coating in our work can be cycled at both elevated current density of 2 mA cm⁻² and elevated capacity of 2 mAh cm⁻², which is still rarely reported to date in the system using the carbonate-based electrolyte. A plating/stripping capacity over 1 mAh cm⁻² for artificial SEI in planer Li foil is considered challenging to realize due to the large volume expansion, while a high capacity of 3 mAh cm⁻² can be applied in Li@H10 for 350 h in this work. The cycling performance at higher current density is believed to be further improved if the HPU artificial interphase is applied to the 3D host. The electrochemical impedance spectroscopy (EIS) was further tested to evaluate the interfacial resistance

of Li metal anodes, as shown in Figure S10 in the Supporting Information. In the Nyquist plots of bare Li and Li@H10 before cycling, the interfacial resistance of Li@H10 is higher than bare Li due to the non-ionic conductive nature of HPU. However, after ten electrochemical cycles, the interfacial resistance of Li@H10 became considerably smaller than bare Li, indicating the lithiation process of the HPU during the initial cycles. The lithiation phenomenon in HPU we observed in this work is similar to PU as we previously reported.^[18] Coulombic efficiency (CE), defined as the ratio of the Li stripping capacity to Li plating capacity for each cycle, is a critical factor to evaluate the cycling stability and predict the cycle life of Li metal anode.^[29] We applied Cu foil either with or without HPU coating as working electrodes and Li foils as counter electrodes to evaluate the CEs. The electrolyte was 1 M bis(trifluoromethanesulfonyl) imide (LiTFSI) in DME/DOL (1:1 v/v) with 1 wt% LiNO₃. Figure 2C shows the CE testing at a current density of 0.5 mA cm⁻² for a capacity of 0.5 mAh cm⁻². For bare Cu the CE dropped to below 90% after 150 cycles, whereas Cu@H10 retained a high CE of ≈98% without obvious decrease throughout the test for 500 cycles. When increasing both current density and capacity to 1 mA cm⁻² and 1 mAh cm⁻² respectively, Cu@H10 still exhibited prolonged

cycle life with stable CE for 450 cycles, which is more than 4 times the lifespan of bare Cu (Figure 2D).

To study the effect of HPU coatings on the cycling stability improvement, the morphology of bare Li and Li@H10 after 20 charge/discharge cycles are characterized by scanning electron microscopy (SEM). On the cross-section image of bare Li (Figure S11A, Supporting Information) a thick layer of ≈90 μm “dead Li” was clearly observed on the top of the bulk Li. Porous structure of Li due to huge volume expansion and contraction during charge/discharge is shown in the higher magnified image (Figure S11B, Supporting Information). On the top-view image (Figure 3A) the irregular structures indicated that non-uniform Li plating/stripping occurred during the electrochemical process. Large amount of mossy-like Li is presented in the enlarged area as shown in Figure 3B. Such irregular Li structures will continue to accumulate on the further plating/stripping process, increase the polarization on the interface and accelerate the failure of the cells. Li@H10 in Figure S11C in the Supporting Information, by contrast, did not exhibit obvious layer of dead Li after electrochemical cycling. The electrode surface of Li@H10 in the cross-section was much flatter than bare Li. From top-view in Figure 3C,D, the surface of Li@H10 was very smooth and the formation of dendritic or mossy-like

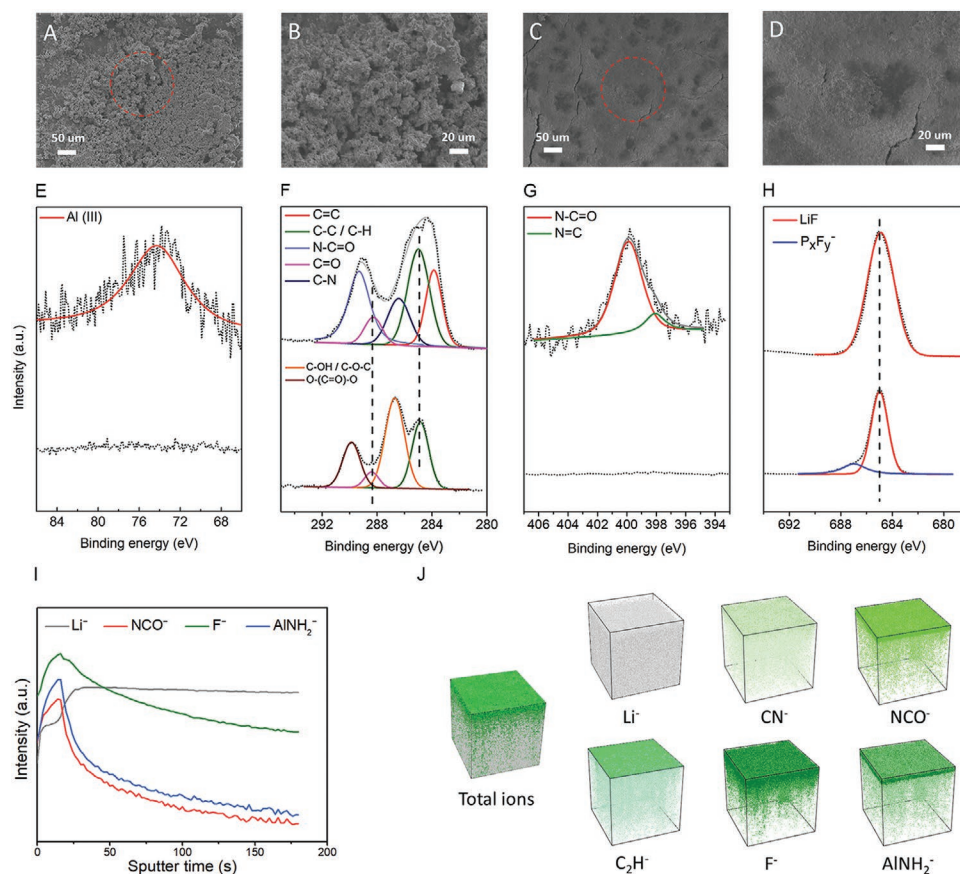


Figure 3. Characterization on the electrode surface of bare Li and Li@H10 after 20 charge/discharge cycles from symmetric cells. SEM top-view images of A) bare Li and B) corresponding magnified image of highlighted area by dotted line. SEM top-view images of C) Li@H10 and D) corresponding magnified image of highlighted area by dotted line. High-resolution XPS spectra of bare Li (on the bottom) and Li@H10 (on the top) for E) Al 2p, F) C 1s, G) N 1s, and H) F 1s. I) TOF-SIMS profile depth profile of some typical secondary ions from Li@H10 after 20 charge/discharge cycles. J) 3D reconstruction of various secondary ions after Bi₃⁺ sputtering.

structures in bare Li was not observed. In addition, Li@Al₂O₃@P10 anode was also electrochemically cycled for SEM characterization of comparison (Figure S12, Supporting Information). Although in its cross-section the Li was much more dense and uniform than bare Li, some dendritic Li can still be observed in the higher magnified image. In the top-view images there were severe cracks on the surface, which were the preferred spots for the growth and propagation of dendritic Li as shown in Figure S12F in the Supporting Information. The SEM characterizations also demonstrated Li metal anode with HPU has a highly robust SEI upon electrochemical cycling.

To investigate the chemistry on the interface upon electrochemical cycling, we performed high-resolution X-ray photoelectron spectroscopy (XPS) on both bare Li and Li@H10 after 20 plating/stripping cycles. In the Al 2p spectrum (Figure 3E) the peak at 74.6 eV remained intact as we observed in Li@H10 before electrochemical cycling, indicating again the excellent stability of the MLD HPU thin film. The C 1s spectra are fitted using the peak at 284.8 eV from C–C and C–H (Figure 3F).^[30] For bare Li after cycling, the distinct peaks at 286.7 and 289.9 eV are assigned to C–O and O–(C=O)–O, respectively. Therefore, the major components of SEI on bare Li are the reduced organic products of alkyl carbonates (ROCOOLi) and lithium alkoxides (ROLi). Inorganic Li₂CO₃ could also contribute a small portion of the detected carbonate species. The detected SEI component agrees well with reported results from the literature.^[6] For Li@H10, the peak at 289.3 and 283.8 eV were assigned to N–C=O and C=C, respectively. These species were exclusively from the urea bond and benzene ring, and had no obvious change compared with the C 1s spectrum of Li@10 before cycling. These results suggest that the chemical structure of HPU was well preserved after repeated plating/stripping, and the reduction of organic electrolytes was suppressed by this robust artificial interphase. In N 1s spectrum (Figure 3G), the peak at 399.7 eV from urea bond and the other peak at 398.0 eV from isocyanate end groups both remained. Accordingly, no signal of N was present from bare Li, as N in Li@H10 is introduced from the MLD process. Both Li_xF_y and LiF SEI products were observed in bare Li from F 1s spectrum (Figure 3H). Interestingly, in Li@H10 nearly all the F is in the form of LiF, which is a preferred SEI component because of its high modulus that is sufficient to suppress dendrite growth.^[2,31] This percentage of LiF in Li@H10 is higher than that of pure polyurea coated Li as we reported previously.^[18] Here we propose the mechanism to explain this observation. The formation of LiF on the interphase is from the decomposition of LiPF₆ with trace amount of water due to its hydroscopic property, and hydrogen fluoride (HF) is another reaction product.^[6] The amine groups in polyurea and PF₆[−] can form hydrogen bonds (N–H–F), thus the formation of LiF on the surface of Li can be facilitated. Moreover, HF as a reaction product can be eliminated by its reaction with Al (III) in HPU, promoting the decomposition of LiPF₆ due to the equilibrium law. XPS was also conducted for Li@Al₂O₃@P10 after electrochemical cycling to compare the surface chemistries. No signal was detected from Al 2p and N 1s spectra in Figure S13 in the Supporting Information. The XPS results revealed that the dual-layer coating has been either damaged or decomposed under the electrochemical process. Compared to Li@Al₂O₃@P10, the artificial SEI of Li@H10 is more mechanically

robust, which also explains its improved electrochemical performance. TOF-SIMS was performed to obtain a detailed depth-profile from secondary ions for the artificial SEI (Figure 3I). The counts of Li[−] gradually increased and became leveled upon sputter for 30 s, which was much quicker than that for uncycled Li@H10 due to the formation of LiF on the surface from XPS data. Species from HPU, including AlNH₂[−] and NCO[−], became almost leveled after continuous decreasing for 150 s. Therefore, the thickness of the artificial SEI was estimated to be ≈30 nm as we consider the sputter rate was approximate ≈0.2 nm s^{−1}. The thickness of SEI did not have a significant change after electrochemical cycling. An illustration of the SEI on the surface of Li is shown in Figure 3J by the 3D reconstruction of various secondary ions.

To evaluate the protected anodes in real LMB applications, both Li@H10 and bare Li were coupled with lithium iron phosphate (LFP) and air electrodes for Li-LFP and Li–O₂ batteries (Figure 4). The electrolyte in Li-LFP cells is 1 M LiPF₆ in 1:1:1 ethylene carbonate (EC)/diethyl carbonate (DEC)/dimethyl carbonate (DMC) and the areal loading of active material is 4.8 mg cm^{−2}. The cross-section SEM image of the LFP cathode showed densely packed LFP particles with an average particle size of ≈300 nm (Figure S14A, Supporting Information). Cycling at a rate of 1C (170 mA g^{−1}), the Li-LFP cell using bare Li exhibited an initial discharge capacity of 136.9 mAh g^{−1} and a rapid capacity decay which started to occur after 90 cycles. The bare Li cell only maintained a capacity of 30.2 mAh g^{−1} after 300 cycles, corresponding to a capacity retention of 22.1% (Figure 4A). In contrast, the Li-LFP battery with Li@H10 delivered a capacity of 139.3 mAh g^{−1} for the 1st cycle and 132.7 mAh g^{−1} after 300 cycles, exhibiting a much higher capacity retention of 95.2% with a negligible decay throughout the test, and the performance is improved compared with Li@P10 as we reported previously even with lower mass loading of LFP.^[19] Detailed charge-discharge profile in Figure 4B showed a much lower polarization of Li@H10 than bare Li after 150 cycles. The testing results in Li-LFP cells indicated the protection on Li metal anode by HPU is effective for improved performance in full cells. We also tested the cycling performance of Li–O₂ batteries using a nitrogen-doped carbon nanotubes/carbon paper (NCNT/CP) composite as the cathode, as previously reported.^[32] SEM image of the composite cathode in Figure S14B in the Supporting Information clearly showed that the surface on carbon fibers of CP are densely covered by NCNT. The average length of NCNT can be observed to be ≈30 μm in the higher magnification image (Figure S14C, Supporting Information). The cycling capacity of 0.1 mAh cm^{−2} can be maintained for more than 300 charge/discharge cycles with Li@H10 in Figure 4D. The Li–O₂ battery with Li@H10 as anode showed a prolonged lifetime for more than 600 h, whereas the Li–O₂ battery with bare Li just delivered a short cycling life of 100 h with fluctuating voltage polarizations (Figure 4C). With Li@H10, very stable voltage profiles at 1st cycle and 30th cycle were observed, while that with bare Li exhibited serious soft short circuits as indicated by the intensive fluctuation in the voltage profile. We demonstrate that the challenges in Li–O₂ batteries, such as oxygen species crossover and dendrite growth, can also be efficiently mitigated through this artificial interphase on Li.

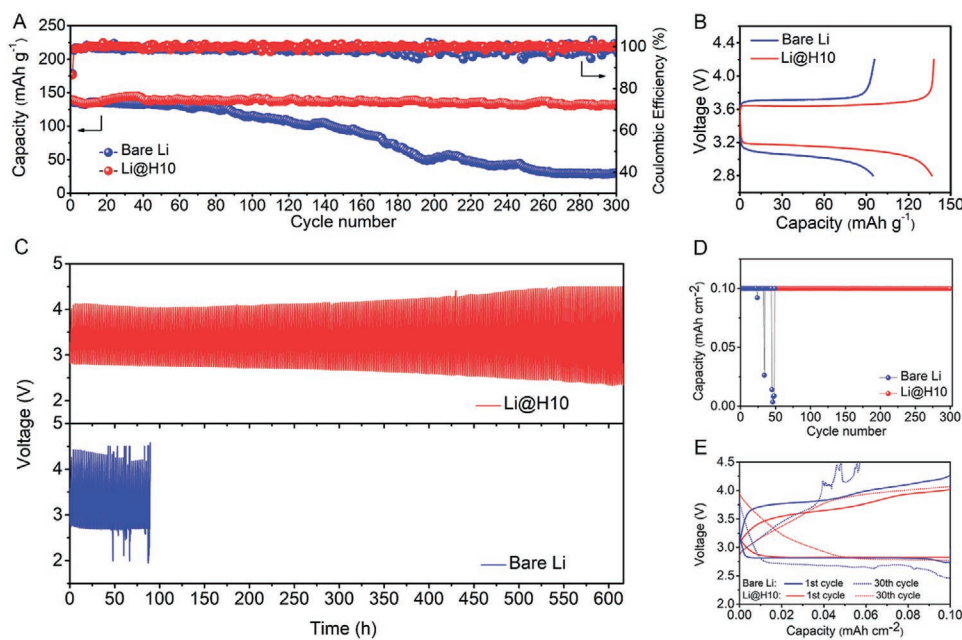


Figure 4. A) Cycling performance of Li-LFP cells at a rate of 1C (170 mA g⁻¹) using bare Li and Li@H10. B) Corresponding galvanostatic charge/discharge curve after 150 cycles. C) Electrochemical performance of Li-O₂ battery with Li@H10 and bare Li. D) Corresponding capacity comparison. E) Discharge/charge profiles at 1st cycle and 30th cycle.

3. Conclusion

In summary, we have demonstrated that MLD hybrid inorganic-organic polyurea coating can produce a stable artificial SEI for high performance Li metal anodes. By precise control over the film composition via MLD, HPU with enhanced stiffness leads to protected Li metal anode that can be operated at high current density (5 mA cm⁻²) and high capacity (2 mAh cm⁻²) with negligible increase in overpotential. Compared to bare Li, the dendrite growth is efficiently suppressed, and the amount of dead Li is minimized by the artificial SEI. Due to the rational design of the protective film on Li, highly improved electrochemical performance is achieved in both Li-LFP and Li-O₂ cells. We believe our approach to building nanoscale artificial SEI can create more possibilities toward high performance energy-storage systems.

Supporting Information

Supporting Information is available from the Wiley Online Library or from the author.

Acknowledgements

This research was supported by the Natural Science and Engineering Research Council of Canada (NSERC), the Canada Research Chair Program (CRC), the Canada Foundation for Innovation (CFI), General Motors R&D Center, Ontario Research Fund (ORF), and the University of Western Ontario (UWO). The authors would also like to acknowledge the help of beamline staff at the Spherical Grating Monochromator

(SGM) of the Canadian Light Source (CLS). T.F. acknowledges funding by The Ontario Ministry of Research, Innovation Early Researcher, the Erwin Edward Hart Professorship, NSERC and CFI. The authors gratefully acknowledge Dr. Heng-Yong Nie for his help in the discussion on TOF-SIMS results. Y.Z. appreciates the funding support of Mitacs Elevate Postdoctoral Fellowship.

Conflict of Interest

The authors declare no conflict of interest.

Author Contributions

Y.S. and M.A. contributed equally to this work. X.S., T.-K.S., M.C., and T.F. supervised the whole project. Y.S. prepared the coatings, tested the electrochemical performance, and wrote the manuscript. M.A., T.C., and G.W. conducted the AFM measurements, modulus calculation, and wrote the relevant part. Y.Z. and Y.S. performed material characterizations. C.Z. prepared the air electrode for Li-O₂ batteries. J.L. and C.W. prepared the LFP cathodes. K.R.A. and Y.S. conducted the NEXAFS measurements. J.L. carried out ICP test. R.L. interpreted the experimental results. All authors read and commented on the manuscript.

Keywords

Li-metal anodes, mechanical properties, rechargeable batteries, solid-electrolyte interphases, thin films

Received: March 31, 2020

Revised: May 2, 2020

Published online:

- [1] a) Z. W. Seh, Y. Sun, Q. Zhang, Y. Cui, *Chem. Soc. Rev.* **2016**, *45*, 5605; b) D. Lin, Y. Liu, Y. Cui, *Nat. Nanotechnol.* **2017**, *12*, 194; c) B. Liu, J.-G. Zhang, W. Xu, *Joule* **2018**, *2*, 833.
- [2] M. D. Tikekar, S. Choudhury, Z. Tu, L. A. Archer, *Nat. Energy* **2016**, *1*, 16114.
- [3] a) X.-B. Cheng, R. Zhang, C.-Z. Zhao, Q. Zhang, *Chem. Rev.* **2017**, *117*, 10403; b) B. Yao, S. Chandrasekaran, J. Zhang, W. Xiao, F. Qian, C. Zhu, E. B. Duoss, C. M. Spadaccini, M. A. Worsley, Y. Li, *Joule* **2019**, *3*, 459.
- [4] a) Y. Zhao, X. Yang, Q. Sun, X. Gao, X. Lin, C. Wang, F. Zhao, Y. Sun, K. R. Adair, R. Li, M. Cai, X. Sun, *Energy Storage Mater.* **2018**, *15*, 415; b) K. N. Wood, M. Noked, N. P. Dasgupta, *ACS Energy Lett.* **2017**, *2*, 664.
- [5] W. Xu, J. Wang, F. Ding, X. Chen, E. Nasybulin, Y. Zhang, J.-G. Zhang, *Energy Environ. Sci.* **2014**, *7*, 513.
- [6] X.-B. Cheng, R. Zhang, C.-Z. Zhao, F. Wei, J.-G. Zhang, Q. Zhang, *Adv. Sci.* **2016**, *3*, 1500213.
- [7] Y. Gao, Z. Yan, J. L. Gray, X. He, D. Wang, T. Chen, Q. Huang, Y. C. Li, H. Wang, S. H. Kim, T. E. Mallouk, D. Wang, *Nat. Mater.* **2019**, *18*, 384.
- [8] a) V. Kumar, Y. Wang, A. Y. S. Eng, M.-F. Ng, Z. W. Seh, *Cell Rep. Phys. Sci.* **2020**, *1*, 100044; b) V. Kumar, A. Y. S. Eng, Y. Wang, D.-T. Nguyen, M.-F. Ng, Z. W. Seh, *Energy Storage Mater.* **2020**, *29*, 1.
- [9] F. Ding, W. Xu, G. L. Graff, J. Zhang, M. L. Sushko, X. Chen, Y. Shao, M. H. Engelhard, Z. Nie, J. Xiao, X. Liu, P. V. Sushko, J. Liu, J.-G. Zhang, *J. Am. Chem. Soc.* **2013**, *135*, 4450.
- [10] X.-Q. Zhang, X.-B. Cheng, X. Chen, C. Yan, Q. Zhang, *Adv. Funct. Mater.* **2017**, *27*, 1605989.
- [11] R. Weber, M. Genovese, A. J. Louli, S. Harnes, C. Martin, I. G. Hill, J. R. Dahn, *Nat. Energy* **2019**, *4*, 683.
- [12] Y. Liu, J. Liu, J. Wang, M. N. Banis, B. Xiao, A. Lushington, W. Xiao, R. Li, T.-K. Sham, G. Liang, X. Sun, *Nat. Commun.* **2018**, *9*, 929.
- [13] N.-W. Li, Y.-X. Yin, C.-P. Yang, Y.-G. Guo, *Adv. Mater.* **2016**, *28*, 1853.
- [14] a) Q. Li, F.-L. Zeng, Y.-P. Guan, Z.-Q. Jin, Y.-Q. Huang, M. Yao, W.-K. Wang, A.-B. Wang, *Energy Storage Mater.* **2018**, *13*, 151; b) J. Luo, C.-C. Fang, N.-L. Wu, *Adv. Energy Mater.* **2018**, *8*, 1701482.
- [15] a) A. C. Kozen, C.-F. Lin, A. J. Pearce, M. A. Schroeder, X. Han, L. Hu, S.-B. Lee, G. W. Rubloff, M. Noked, *ACS Nano* **2015**, *9*, 5884; b) E. Kazyak, K. N. Wood, N. P. Dasgupta, *Chem. Mater.* **2015**, *27*, 6457; c) L. Chen, J. G. Connell, A. Nie, Z. Huang, K. R. Zavadil, K. C. Klavetter, Y. Yuan, S. Sharifi-Asl, R. Shahbazian-Yassar, J. A. Libera, A. U. Mane, J. W. Elam, *J. Mater. Chem. A* **2017**, *5*, 12297.
- [16] P. K. Alaboina, S. Rodrigues, M. Rottmayer, S.-J. Cho, *ACS Appl. Mater. Interfaces* **2018**, *10*, 32801.
- [17] a) Y. Zhao, K. Zheng, X. Sun, *Joule* **2018**, *2*, 2583; b) Y. Zhao, X. Sun, *ACS Energy Lett.* **2018**, *3*, 899.
- [18] Y. Sun, Y. Zhao, J. Wang, J. Liang, C. Wang, Q. Sun, X. Lin, K. R. Adair, J. Luo, D. Wang, R. Li, M. Cai, T.-K. Sham, X. Sun, *Adv. Mater.* **2019**, *31*, 1806541.
- [19] F. Han, A. S. Westover, J. Yue, X. Fan, F. Wang, M. Chi, D. N. Leonard, N. J. Dudney, H. Wang, C. Wang, *Nat. Energy* **2019**, *4*, 187.
- [20] A. Lushington, C. Langford, J. Liu, K. Nie, R. Li, X. Sun, J. Guo, X. Sun, *J. Phys. Chem. C* **2017**, *121*, 11757.
- [21] I. Iatsunskiy, M. Kempirski, M. Jancelewicz, K. Załęski, S. Jurga, V. Smyntyna, *Vacuum* **2015**, *113*, 52.
- [22] S. G. Urquhart, A. P. Hitchcock, R. D. Priestler, E. G. Rightor, *J. Polym. Sci., Part B: Polym. Phys.* **1995**, *33*, 1603.
- [23] R. R. Cooney, S. G. Urquhart, *J. Phys. Chem. B* **2004**, *108*, 18185.
- [24] P. Leinweber, J. Kruse, F. L. Walley, A. Gillespie, K.-U. Eckhardt, R. I. R. Blyth, T. Regier, *J. Synchrotron Radiat.* **2007**, *14*, 500.
- [25] C. Cao, S. Mukherjee, J. Liu, B. Wang, M. Amirmaleki, Z. Lu, J. Y. Howe, D. Perovic, X. Sun, C. V. Singh, Y. Sun, T. Filleter, *Nanoscale* **2017**, *9*, 11678.
- [26] a) A. Castellanos-Gomez, M. Poot, G. A. Steele, H. S. J. van der Zant, N. Agraït, G. Rubio-Bollinger, *Adv. Mater.* **2012**, *24*, 772; b) S. Timoshenko, *Theory of Plates and Shells*, McGraw-Hill, New York **1959**.
- [27] a) M. Amirmaleki, C. Cao, B. Wang, Y. Zhao, T. Cui, J. Tam, X. Sun, Y. Sun, T. Filleter, *Nanoscale* **2019**, *11*, 18730; b) T. Cui, S. Mukherjee, C. Cao, P. M. Sudeep, J. Tam, P. M. Ajayan, C. V. Singh, Y. Sun, T. Filleter, *Carbon* **2018**, *136*, 168.
- [28] L. Anand, N. M. Ames, *Int. J. Plast.* **2006**, *22*, 1123.
- [29] B. D. Adams, J. Zheng, X. Ren, W. Xu, J.-G. Zhang, *Adv. Energy Mater.* **2018**, *8*, 1702097.
- [30] Z. W. Seh, J. Sun, Y. Sun, Y. Cui, *ACS Cent. Sci.* **2015**, *1*, 449.
- [31] a) D. Lin, Y. Liu, W. Chen, G. Zhou, K. Liu, B. Dunn, Y. Cui, *Nano Lett.* **2017**, *17*, 3731; b) C. Xu, Z. Ahmad, A. Aryanfar, V. Viswanathan, J. R. Greer, *Proc. Natl. Acad. Sci. USA* **2017**, *114*, 57.
- [32] H. Yadegari, M. N. Banis, B. Xiao, Q. Sun, X. Li, A. Lushington, B. Wang, R. Li, T.-K. Sham, X. Cui, X. Sun, *Chem. Mater.* **2015**, *27*, 3040.